Possible use of spin-vortex-induced loop currents as qubits: a numerical simulation for two-qubit system

Hikaru Wakaura, Hiroyasu Koizumi

*Division of Materials Science, University of Tsukuba,Tsukuba, Ibaraki 305-8573, Japan**

(Dated: January 28, 2016)

Abstract

We propose new qubits; they are nano-sized persistent loop currents called, the *spin-vortex-induced loop currents* (SVILCs), predicted to exist in hole doped cuprate superconductors in one of the proposed mechanisms of the cuprate superconductivity. In the SVILC theory for the cuprate superconductivity, the superconducting state arises when the network of SVILCs generates a macroscopic current as a collection of the loop currents.

The predicted SVILC has a number of properties that are suitable for qubits: each SVILC is characterized by topological winding number, thus, expected to be robust against environmental perturbations; because of the smallness of their size, they can be assembled into a large qubit-number system in a small space.

Energy levels of different current patterns of the SVILC system are split by an external inhomogeneous magnetic field, and they are used as qubit states. The quantum gate control is achieved by the Rabi oscillation using electric dipole transitions. We have calculated the transition dipole moments between different SVILC qubit states. Some of the calculated values are relatively large, around 10^{-30} Cm. We have also performed a numerical simulation for the Glover's search algorithm using the two-qubit SVILC system. The search completes in a nanosecond order using the electromagnetic field with electric field amplitude 10^5 V/m. The present results indicate the quantum gate control capability of the SVILC qubits, and suggest the potentiality to satisfy DiVincenzo's criteria for quantum computers.

PACS numbers: 03.67.Lx,42.50.Dv

*s14301131@u.tsukuba.ac.jp; koizumi@ims.tsukuba.ac.jp

I. INTRODUCTION

The physical realization of quantum computers has been a subject of intensive research since the manipulation of quantum superpositioned states that is necessary for the quantum gate control was proved to be feasible [1–3]. However, the realization of programable universal gate type quantum computers must clear a number of hurdles. One of the important issues is the selection of qubits. From the view point of scalability, solid state qubits are attractive. Especially, superconducting qubits are convenient since they can be incorporated into electric circuits [4]. In this respect, it is noteworthy that a quantum annealing computer using superconducting flux qubits is currently available [5].

The performance of qubits are often estimated in terms of the following five criteria presented by DiVincenzo [6]: 1) Initialization capability; 2) Readout capability; 3) Quantum coherence duration; 4) Gate-operation capability; 5) Scalability. No qubit has satisfied the above five criteria so far. In other words, the realization of practical quantum computers is still in the stage of searching for good qubits.

In the present work, we propose qubits that potentially satisfy the above five criteria. They are nano-sized persistent loop currents, called, 'spin-vortex-induced loop currents (SVILCs)', predicted to exist in cuprates by one of the proposed mechanisms for the cuprate superconductivity [7–10]. Although the direct observation of SVILCs has not been achieved, yet, there a number of experimental results that indicate the presence of loop currents and suggest the relevance of the SVILC in the cuprate superconductivity: 1) The hourglass-shaped magnetic excitation observed in the neutron scattering experiment [11] is explained as due to the spin-wave excitation in the presence of spin-vortices in the antiferromagnetic background [7]; 2) The stripe configuration observed in the cuprate [12] is regarded as the linear arrangement of the spin-vortices [7]; 3) Kerr rotation experiment [13], Nernst effect measurement [14], and Neutron scattering measurement indicate the existence of loop currents in the pseudogap phase [15].

The SVILCs are predicted to exist in the CuO_2 plane with doped holes as their cores. The holes in the bulk at low temperature are expected to be rather immobile due to the small polaron formation as is observed by the EXAFS experiment [16] and supported by the theoretical calculation [17]; in this respect, the ARPES experiment that indicates mobile holes should be considered to reflect the surface electronic state. In the SVILC theory

for the cuprate superconductivity, the low temperature bulk electric current is generated by the network of SVILCs made by $4a \times 4a$-sized 'spin-vortex quartet' as a unit (a is the lattice constant of the CuO_2 plane) [9]. Actually, the STM experiment has been observing unidirectional superconducting nano regions with width $4a$, and suggesting the percolation transition temperature of them corresponds to T_c [18].

It is also noteworthy that a theoretical estimate of the superconducting transition temperature T_c for the cuprate corresponds to the stabilization temperature of the coherence-length-sized persistent loop currents [19], which actually is realized in the SVILC theory that T_c for the optimally doped sample is obtained as the global stabilization temperature of the SVILCs [10].

In the present work, we explore the possibility for using SVILCs as qubits based on the assumption that SVILCs exist in the cuprate. Our investigation is a theoretical one employing the calculation method developed for SVILC carrying states using a microscopic Hamiltonian [8–10].

Let us list below the reasons that we think SVILC qubits may satisfy the DiVincenzo 's criteria:

1. Initialization can be achieved by cooling the SVILC system; it will put the system in the ground state.

2. Readout of the qubits can be performed by measuring the magnetic field produced by them. It is also possible to perform readout by measuring the response current to feeding currents.

3. Gate-operation time is reasonably short, which will be shown in this work. Quantum coherence duration is not known but may be long enough since the charge fluctuation is suppressed in the cuprate due to the fact that it is a strongly-correlated system. Besides, each qubit is characterized by the topological winding number, its quantum state is robust against environmental perturbations.

4. Couplers between qubits can be constructed by using feeding currents that allow switching on/off of interactions between them.

5. Size of each qubit is about 10 nm; thus, a large number of qubits can be assembled in a very small space.

The research for the readout by measuring the response current to feeding currents mentioned in Item 2, and the construction of couplers between qubits by using feeding currents mentioned in Item 4 are currently underway.

In the present work, we will consider two-qubit SVILC systems and perform a simulation of a quantum computing in order to assess the gate control capability of SVILC qubits. The energy levels of states with different SVILC qubit states are split by applying a non-uniform magnetic field. The transition dipole moments between them are shown to be around 10^{-30} Cm, which is comparable to the transition moment of the hydrogen $1s$-$2p$ transition. The Glover's search algorithm using the SVILC two-qubit system is shown to complete in a nanosecond order using the electromagnetic field with the electric field amplitude 10^5 V/m. Since the quantum coherence duration is expected to be large in superconductors (may be in the order of a microsecond or larger [20]), the SVILC qubits possess a promising property for the quantum gate control.

The organization of the present work is following: we explain how to calculate states with SVILCs in section II. In Section III, the origin of the appearance of SVILCs is remarked. In Section IV, transition dipole moments between different SVILC states for the spin-vortex quartet (SVQ) are calculated, where the SVQ is a stable unit of spin-vortices. In Section V, a couple of SVILC two-qubit systems are proposed, and transition dipole moments for them are calculated. In Sections VI, quantum gate operations for the SVILC qubits by the electric dipole transition are explained. In Section VII a simulation of the Grover's search algorithm is performed. Lastly, we conclude the present work in Section VIII.

II. CALCULATION OF STATES WITH SVILCS IN MAGNETIC FIELD

We start with the following model Hamiltonian for itinerant electrons in the CuO_2 plane of the cuprate,

$$H_{\rm EHFS} = -\sum_{\langle i,j\rangle_1,\sigma} t(c^\dagger_{i\sigma}c_{j\sigma}+c^\dagger_{j\sigma}c_{i\sigma})+U\sum_j c^\dagger_{j\uparrow}c_{j\uparrow}c^\dagger_{j\downarrow}c_{j\downarrow} + J'\sum_{\langle i,j\rangle_h}\hat{\mathbf{S}}_i\cdot\hat{\mathbf{S}}_j + H_{h-h}, \tag{1}$$

where i and j are sites for coppers. SVILCs exit in the CuO_2 plane in the bulk, and we consider a single CuO_2 plane. Oxygens that exist between nearest neighbor coppers are not explicitly taken into account. The sum of $\langle i,j\rangle_1$ in the first term indicates that

the sum is taken over the nearest neighbor pairs. The sum of $\langle i, j\rangle_h$ in the third term indicates that the sum is taken over the electron pairs across the hole occupied sites, where the holes are assumed to form lattice small polarons. $c^\dagger_{j\sigma}$ and $c_{j\sigma}$ are the creation and annihilation operators of electrons at the jth site with the z-axis projection of electron spin σ, respectively; $\hat{\mathbf{S}}_j$ is the spin moment operator at the jth site given by

$$\hat{\mathbf{S}}_j = \frac{1}{2}\sum_{\tau,\tau'} c^\dagger_{j\tau}\boldsymbol{\sigma}_{\tau\tau'}c_{j\tau'} \tag{2}$$

$\boldsymbol{\sigma}$ is the vector of Pauli matrices.

Let us explain each terms in the Hamiltonian in Eq. (1). The first term is the hopping term and the second is the on-site Coulomb repulsion term. The third term is exchange interaction between electrons across hole-occupied sites; this term arises due to the small polaron formation of the doped holes: the molecular orbital cluster calculation result indicates that when the small polaron is formed, $3\mathrm{d}_{x^2-y^2}$ orbital of copper and the surrounding four p_σ orbitals of oxygens form a molecular orbital (which we denote as h) [17], giving the exchange interaction with parameter J' by acting the hole molecular orbital h as the intermediate level. Using the well-known procedure [21], J' is calculated as

$$J' \approx \frac{2t^4_{dh}}{(\epsilon_h - \epsilon_d)^3} \tag{3}$$

where t_{dh} is the transfer integral between the spin-reside copper $\mathrm{d}_{x^2-y^2}$ orbital and the hole orbital h at the hole-occupied site; ϵ_d and ϵ_h are the orbital energies of $\mathrm{d}_{x^2-y^2}$ and h, respectively, [17]. This term stabilizes the spin-vortices. The last term H_{h-h} describes the Coulomb repulsion between holes which suppresses the appearance of next neighbor hole pairs.

The above Hamiltonian is too difficult to solve as it is, thus, we employ the following simplifications [8–10]:

1. In the situation where supercurrent by the SVILCs flows, we assume that doped holes do not move since the hopping of the small polarons is an energy activation process. We simply exclude lattice sites that are occupied by the holes in the sums in Eq. (1). As a consequence, the sum of the second term in the r.h.s. of Eq. (1) is over the sites that are not occupied by the holes. The last term H_{h-h} is omitted since it does not contribute to the energy difference when the hole positions are fixed.

2. We fix the spin-configuration and calculate the electron energy for various current patterns, then, the third term in Eq. (1) gives only a constant energy shift; thus, we omit it.

3. We simplify the Hamiltonian by employing the mean field approximation. Although the cuprates are strongly-correlated materials, what we concern here is the current produced by SVILCs. As will be explained below, it is generated as a whole system motion. In the whole system motion where all electrons move simultaneously, the importance of the correlation effect is reduced. We take into account the correlation effect simply by adopting the reduced value for t due to the correlation (we use $t = 130$ meV, a fitted value to the experiment [22]).

The mean field Hamiltonian we are going to use is given by

$$\begin{aligned} H^{HF}_{\mathrm{EHFS}} &= -t \sum_{\langle i,j\rangle_1,\sigma} \left(c^\dagger_{i\sigma} c_{j\sigma} + c^\dagger_{j\sigma} c_{i\sigma} \right) \\ &+ U \sum_j \left[(\frac{n_j}{2} - S^z_j) c^\dagger_{j\uparrow} c_{j\uparrow} + (\frac{n_j}{2} + S^z_j) c^\dagger_{j\downarrow} c_{j\downarrow} - (S^x_j - iS^y_j) c^\dagger_{j\uparrow} c_{j\downarrow} - (S^x_j + iS^y_j) c^\dagger_{j\downarrow} c_{j\uparrow} \right] \end{aligned} \tag{4}$$

where

$$n_j = \sum_\sigma \langle c^\dagger_{j\sigma} c_{j\sigma} \rangle \tag{5}$$

is the number of electrons at the jth site, and $\mathbf{S}_j = (S^x_j, S^y_j, S^z_j)$ is the electron spin at the jth site given by

$$\begin{aligned} S^x_j &= \frac{1}{2} \langle c^\dagger_{j\uparrow} c_{j\downarrow} + c^\dagger_{j\downarrow} c_{j\uparrow} \rangle = S_j \cos\xi_j \sin\zeta_j \\ S^y_j &= -\frac{i}{2} \langle c^\dagger_{j\uparrow} c_{j\downarrow} - c^\dagger_{j\downarrow} c_{j\uparrow} \rangle = S_j \sin\xi_j \sin\zeta_j \\ S^z_j &= \frac{1}{2} \langle c^\dagger_{j\uparrow} c_{j\uparrow} - c^\dagger_{j\downarrow} c_{j\downarrow} \rangle = S_j \cos\zeta_j \end{aligned} \tag{6}$$

where ξ and ζ are the azimuth and polar angle angles, respectively; $\langle \hat{O} \rangle$ denotes the expectation value of the operator $\hat{O}$. n_j, S^x_j, S^y_j, and S^z_j are obtained self-consistently by diagonalizing the Hamiltonian in Eq. (4). Actually, we found that we can take $\zeta = \pi/2$ for all the sites since the numerical calculations revealed its stability. Thus, the spins are lying in the CuO_2 plane.

The single-particle wave function is expressed as

$$|\gamma\rangle \;=\; \sum_j e^{-i\frac{\chi_j}{2}}[e^{-i\frac{\xi_j}{2}}D^{\gamma}_{j\uparrow}c^{\dagger}_{j\uparrow}+e^{i\frac{\xi_j}{2}}D^{\gamma}_{j\downarrow}c^{\dagger}_{j\downarrow}]|\mathrm{vac}\rangle. \tag{7}$$

The parameters $D^{\gamma}_{j\uparrow}$, $D^{\gamma}_{j\downarrow}$, ξ_j, and χ_j will be obtained numerically, where j is the index of the jth site of the CuO_2 plane. The above wave function is a single-particle wave function for electrons moving with twisting their spin-directions. The spin-twisting is described by the angle ξ, characterized by the winding number of ξ for loop C_ℓ defined by

$$w_\ell[\xi] = \frac{1}{2\pi}\sum_{i=1}^{N_\ell}(\xi_{C_\ell(i+1)} - \xi_{C_\ell(i)}), \tag{8}$$

where N_ℓ is the number of lattice points for loop C_ℓ; $C_\ell(i)$ denotes the ith lattice point in C_ℓ with the boundary condition $C_\ell(N_\ell+1) = C_\ell(1)$.

When the phase factor $e^{\pm\frac{i}{2}\xi_{C_\ell(1)}}$ is evaluated starting from $C_\ell(1)$ by moving along closed path C_ℓ, it becomes

$$e^{\pm\frac{i}{2}(\xi_{C_\ell(1)}+2\pi w_\ell[\xi])} = (-1)^{w_\ell[\xi]}e^{\pm\frac{i}{2}\xi_{C_\ell(1)}} \tag{9}$$

If $w_\ell[\xi]$ is odd, sign change occurs. This means that the wave function $|\gamma\rangle$ in Eq. (7) becomes multi-valued without the phase factor $e^{-i\frac{\chi_j}{2}}$. In other words, the angular variable χ in Eq. (7) is introduced to compensate the sign change, and make $|\gamma\rangle$ single-valued.

The single-valued requirement of the wave function is satisfied by imposing the following constraint on χ;

$$w_\ell[\chi] + w_\ell[\xi] = \text{even for all loops } C_\ell \tag{10}$$

The above constraint is taken into account by using the following functional,

$$F[\nabla\chi] = E[\nabla\chi] + \sum_{\ell=1}^{N_{\mathrm{loop}}}\lambda_\ell\left(\oint_{C_\ell}\nabla\chi\cdot d\mathbf{r} - 2\pi\bar{w}_\ell\right), \tag{11}$$

where $E[\nabla\chi]$ is the total energy depends on $\nabla\chi$; the second term is the one arising from the constraint with λ_ℓ being the Lagrange multiplier; $\bar{w}_\ell$ is the winding number of χ along loop C_ℓ that satisfies the constraint in Eq. (10); N_{loop} is the number of independent loops, where any loop in the system can be constructed by combining the N_{loop} independent loops.

A set of values for $\bar{w}_\ell$ in Eq. (11) specifies a particular current distribution; namely, by changing the values of $\bar{w}_\ell$ for the independent loops, solutions with different current

distributions are obtained. In the following, we obtain states with different current patterns by changing $\nabla\chi$ only (values for $D^{\gamma}_{j\downarrow}$ and ξ_j are fixed).

Due to the phase factor $e^{-i\frac{\chi_j}{2}}$ in Eq. (7), the superconducting wave function is given in the following form

$$\Psi(\mathbf{r}^{(1)},\cdots,\mathbf{r}^{(N)}) = \Psi_0(\mathbf{r}^{(1)},\cdots,\mathbf{r}^{(N)})e^{-\frac{i}{2}\sum_{\alpha=1}^{N}\chi(\mathbf{r}^{(\alpha)})} \tag{12}$$

where $\mathbf{r}^{(\alpha)}$ is the coordinate of the αth electron and N is the total number of electrons. Ψ_0 is a currentless multi-valued wave function, where the multi-valuedness arises from the spin-twisting of the itinerant electrons.

From the stationary condition of $F[\nabla\chi]$, $\nabla\chi$ is obtained as the solution of

$$0 = \frac{\delta F[\nabla\chi]}{\delta\nabla\chi} = \frac{\delta E[\nabla\chi]}{\delta\nabla\chi} + \sum_{\ell=1}^{N_{\rm loop}} \lambda_\ell \frac{\delta}{\delta\nabla\chi}\oint_{C_\ell}\nabla\chi\cdot d\mathbf{r} \tag{13}$$

with the constraint,

$$\oint_{C_\ell}\nabla\chi\cdot d\mathbf{r} - 2\pi\bar{w}_\ell = 0 \text{ for all independent loops } C_\ell. \tag{14}$$

A method to solve the system of equations composed of Eq. (13) and Eq. (14) will be found in our previous works [8, 9].

III. REMARKS ON THE ORIGIN OF SVILCS

When spin-vortices are created by itinerant electrons, singularities of the wave function arise at the centers of the spin-vortices. Such singularities were not handled properly for a long time, but a method to deal with them have been developed [8, 9]. SVILCs appear when these singularities arise. In this situation, the simple energy minimization yields wave functions (they correspond to Ψ_0 in Eq. (12)) that are multi-valued around the singularities. In other words, Ψ_0 becomes multi-valued due to the spin-twisting itinerant motion. In this situation, the single-valued requirement must be imposed in addition to the energy minimization. In our method, this requirement is achieved by introducing the phase factor $e^{-\frac{i}{2}\sum_{\alpha=1}^{N}\chi(\mathbf{r}^{(\alpha)})}$ in Ψ of Eq. (12); note that Mead and Truhlar handled a similar sign-change problem with an analogous method [23].

Due to this phase factor, $E[\nabla\chi]$ is expressed as

$$E[\nabla\chi] = \langle\Psi|H^{HF}_{\rm EHFS}[\mathbf{A}^{\rm em}]|\Psi\rangle = \langle\Psi_0|H^{HF}_{\rm EHFS}[\mathbf{A}^{\rm em} - \frac{c\hbar}{2e}\nabla\chi]|\Psi_0\rangle = E^{\rm super}[\mathbf{A}^{\rm em} - \frac{c\hbar}{2e}\nabla\chi], \tag{15}$$

where $H^{HF}_{\rm EHFS}[\mathbf{A}^{\rm em}]$ is the Hamiltonian $H^{HF}_{\rm EHFS}$ with the electromagnetic vector potential $\mathbf{A}^{\rm em}$ included, and $E^{\rm super}[\mathbf{A}^{\rm em} - \frac{c\hbar}{2e}\nabla\chi]$ is the energy functional that depends on $\mathbf{A}^{\rm em}$ and $\nabla\chi$.

The current density is expressed using the energy functional as

$$\mathbf{j} = -c\frac{\delta E^{\rm super}[\mathbf{A}^{\rm em} - \frac{c\hbar}{2e}\nabla\chi]}{\delta \mathbf{A}^{\rm em}} = \frac{2e}{\hbar}\frac{\delta E^{\rm super}[\mathbf{A}^{\rm em} - \frac{c\hbar}{2e}\nabla\chi]}{\delta\nabla\chi} = \frac{2e}{\hbar}\frac{\delta E[\nabla\chi]}{\delta\nabla\chi}, \tag{16}$$

where the fact is used that $\mathbf{A}^{\rm em}$ appears in the combination

$$\mathbf{A}^{\rm em} - \frac{c\hbar}{2e}\nabla\chi \tag{17}$$

in the energy functional.

Using Eq. (13), the current density is given by

$$\mathbf{j} = -\frac{2e}{\hbar}\sum_{\ell=1}^{N_{\rm loop}} \lambda_\ell \frac{\delta}{\delta\nabla\chi}\oint_{C_\ell} \nabla\chi\cdot d\mathbf{r}. \tag{18}$$

This indicates that the current is generated by the phase factor $e^{-\frac{i}{2}\sum_{\alpha=1}^{N}\chi(\mathbf{r}^{(\alpha)})}$ in a non-perturbative way. The current is a sum of loop currents, 'spin-vortex-induced loop-currents (SVILCs)'. This current can be obtained either by evaluating λ_ℓ's or calculating the expectation value of the current density operator with the wave function in Eq. (12) [9].

Each SVILC is protected by the topological constraint given in Eq. (14); thus, they will be robust against perturbations from the environment.

IV. TRANSITION DIPOLE MOMENTS OF SPIN VORTEX QUARTET STATES

In the following calculations, we use the lattice constant of the CuO_2 plane, $a = 0.4$ nm, the transfer integral, $t = 130$ meV, and the Coulomb repulsion parameter, $U = 8t$ [22].

We apply a magnetic field and remove the degeneracy of SVILC states. The perturbation for it is given by

$$H_{\rm B} = -\sum_{\langle k,j\rangle_1}\int_{\boldsymbol{r}_j}^{\boldsymbol{r}_k} \mathbf{A}^{\rm em}(\boldsymbol{r})\cdot d\boldsymbol{r}\hat{j}_{k\leftarrow j}, \tag{19}$$

where $\hat{j}_{k\leftarrow j}$ is the current operator for the current from site j to its nearest neighbor site k given by

$$\hat{j}_{k\leftarrow j} = ie\hbar^{-1}t\sum_\sigma (c^\dagger_{k\sigma}c_{j\sigma} - c^\dagger_{j\sigma}c_{k\sigma}). \tag{20}$$

The coordinates for sites j and k are denoted as $\boldsymbol{r}_j$ and $\boldsymbol{r}_k$, respectively.

We obtain wave functions for different SVILC states, which we denote as $\tilde{\Phi}_a$, where a indicates the current pattern specified by the winding numbers. A set of total electronic wave functions $\{|\tilde{\Phi}_a\rangle\}$ obtained forms a non-orthonormal basis. From this, we construct an orthogonal basis $\{|\Phi_a\rangle\}$ by diagonalizing the matrix for the operator $H_{\rm B}$ whose (a,b) element is given by $\langle\tilde{\Phi}_a|H_{\rm B}|\tilde{\Phi}_b\rangle$. This orthogonal basis is used for the simulation of quantum computations.

Strictly speaking, we should use the basis that diagonalizes the total Hamiltonian $H^{HF}_{\rm EHFS}+H_{\rm B}$. However, the quality of the approximate wave function $\tilde{\Phi}_a$ is not very good; it is not close to the one satisfying the eigenvalue relation,

$$H^{HF}_{\rm EHFS}[\mathbf{A}^{\rm em}-\frac{c\hbar}{2e}\nabla\chi]|\Psi_0\rangle=\bar{E}|\Psi_0\rangle, \tag{21}$$

where $\bar{E}$ is the energy eigenvalue. We have not succeeded in developing the way to improve the quality the wave functions, so far; for now, we are content to use the basis $\{|\Phi_a\rangle\}$ by adopting $\langle\Phi_a|H^{HF}_{\rm EHFS}+H_{\rm B}|\Phi_a\rangle$ as the energy for the state $|\Phi_a\rangle$. The improvement of the quality of the wave function will be a future problem.

Quantum superposition states are constructed using electric dipole transitions. The interaction Hamiltonian for the dipole transition is given by

$$H_D=-\sum_j e(c^\dagger_{j\uparrow}c_{j\uparrow}+c^\dagger_{j\downarrow}c_{j\downarrow})\mathbf{r}_j\cdot\mathbf{e}\mathcal{E}_0\cos\omega t \tag{22}$$

where $\mathbf{e}\mathcal{E}_0\cos\omega t$ is the electric field of the applied radiation and $\mathbf{r}_j=(x_j,y_j,0)$ is the coordinate of the jth site. $\mathbf{e}$ is the polarization vector of the radiation.

The matrix element of H_D between Φ_k and Φ_l is given by

$$\langle\Phi_k\mid H_D\mid\Phi_l\rangle=\mathcal{E}_0(\mu^x_{kl}\cos\alpha+\mu^y_{kl}\sin\alpha)\cos\omega t \tag{23}$$

where x and y components of the transition dipole are given by

$$\mu^x_{kl}\;=\;-\sum_j e(c^\dagger_{j\uparrow}c_{j\uparrow}+c^\dagger_{j\downarrow}c_{j\downarrow})x_j \tag{24}$$

and

$$\mu^y_{kl}\;=\;-\sum_j e(c^\dagger_{j\uparrow}c_{j\uparrow}+c^\dagger_{j\downarrow}c_{j\downarrow})y_j, \tag{25}$$

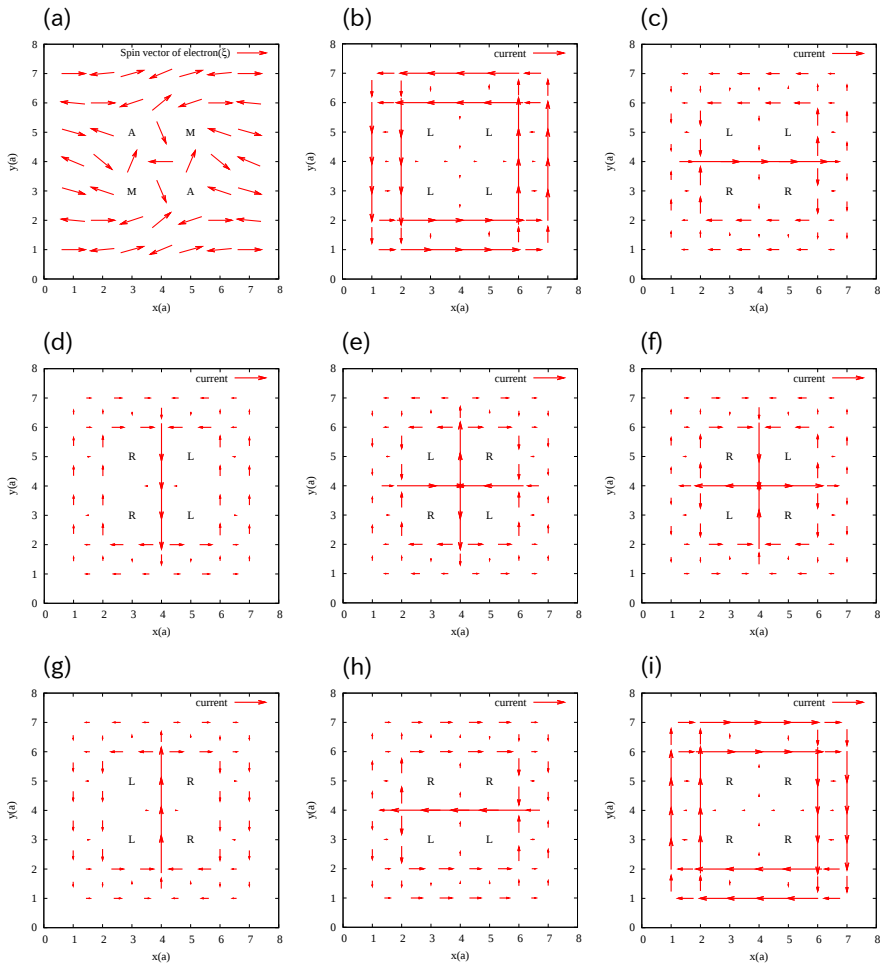

FIG. 1: The spin structure of SVQ and 8 current patterns may be used for qubits. These 8 states are derived by applying a magnetic field in the z direction given by $B = 0.1x + 0.5y$ T (x and y are in nm). a is the lattice constant of CuO_2 plane. (a) Spin structure of SVQ. Arrows on the each lattice point indicates the spin direction of electron whose angle is given by ξ_j. 'M' and 'A' denote spins with $w_l[\xi] = 1$ and $w_l[\xi] = -1$, respectively. (b)-(i) SVILCs depicted by arrows. 'L ' and 'R' denote currents with $w_l[\chi] = 1$ and $w_l[\chi] = -1$, respectively.

respectively; the polarization vector is given by $\mathbf{e} = (\cos\alpha, \sin\alpha, 0)$.

As a unit of spin-vortices, we take 'the Spin-Vortex-Quartet (SVQ)' shown in Fig. 1(a), since it is a stable unit [9]. SVILCs arising from a single SVQ are depicted in Fig. 1(b)-(i). Transition dipole moments between them are tabulated in Table I. Some of them are around 10^{-30} Cm, which is comparable to the transition moment of the hydrogen $1s$-$2p$ transition, indicating that the transition dipole moments are relatively large.

TABLE I: Transition dipole moments between states with different current patterns for the spin-vortex quartet (SVQ). The current patterns are depicted in Fig. 1. The value of the x (y) component is tabulated in the lower-left (upper-right) triangle positions of the table. The units of the moment is 10^{-30} Cm.

		μ^y_{kl}							
	l	L L	L L	R L	R L	L R	L R	R R	R R
	k	L L	R R	R L	L R	R L	L R	L L	R R
μ^x_{kl}	L L L L		0.758	6.297	0.015	0.015	6.036	0.747	0.088
	L L R R	6.708		1.415	0.261	0.261	3.049	0.199	0.747
	R L R L	1.14	8.98		2.14	2.14	36.583	3.049	6.036
	R L L R	0.076	2.139	0.261		0	2.14	0.261	0.015
	L R R L	0.076	2.139	0.261	0		2.14	0.261	0.015
	L R L R	0.372	12.592	2.637	0.261	0.261		1.415	6.297
	R R L L	5.657	29.546	12.592	2.139	2.139	8.98		0.758
	R R R R	0.44	5.657	0.372	0.076	0.076	1.14	6.708	

The magnitude of the transition dipole moment is related to the transition charge density defined as

$$\rho_k{}^{ij} = \langle \Phi_i \mid (c_{k\uparrow}{}^\dagger c_{k\uparrow} + c_{k\downarrow}{}^\dagger c_{k\downarrow}) \mid \Phi_j \rangle. \tag{26}$$

In Fig. 2, transition charge densities are depicted. It clearly shows that the large value for the x component of the transition between (c) and (h) (and also y component of the transition between (d) and (g)) correlates with the large value for the corresponding transition charge

density.

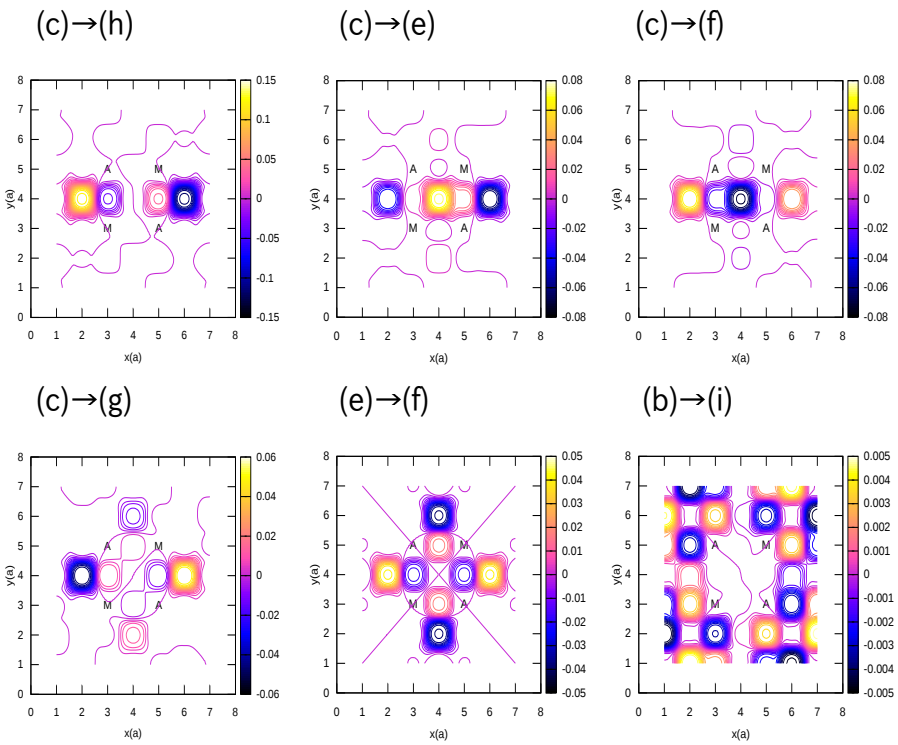

FIG. 2: Imaginary part of transition charge density divided by e for the SVQ system. In our calculations, Real part is calculated to be zero for all transitions. Large dipole transitions correspond to large transition charge density. For example, for x component of the transition dipole moment between (c) and (h) states in Fig. 1 is very large.

V. TRANSITION DIPOLE MOMENTS OF SPIN-VORTEX-INDUCED LOOP CURRENTS

According to Table I, the y component of the dipole transition moment between (d) and (g) in Fig. 1 is very large. So the first candidate of qubit is upward directed current and downward directed current depicted in (d) and (g) in Fig. 1. We call it Dipole-Current-Qubit (DCQ). We denote the upward directed current state as $|U\rangle$ and the downward directed current state as $|D\rangle$; they correspond to $|0\rangle$ and $|1\rangle$ states of a qubit, respectively.

As the two-qubit system of DCQs, we consider the system depicted in Fig. 3. We calculate the four state basis of qubits, $|DD\rangle$, $|DU\rangle$, $|UU\rangle$, and $|UD\rangle$, by diagonalizing H_B with the

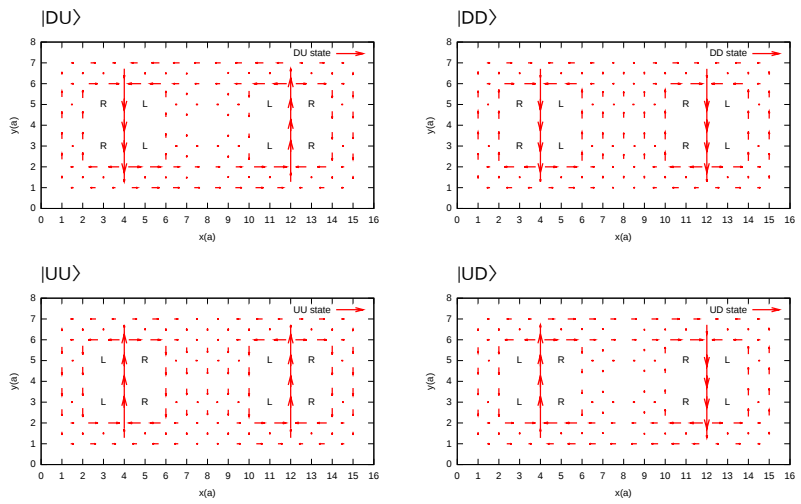

FIG. 3: Four patterns of current states for the two-qubit system of DCQ. They are indicated as $|\,DD\rangle$,$|\,DU\rangle$,$|\,UD\rangle$, and $|\,UU\rangle$.

magnetic flux density in the z direction B given by $B = B_0 x$ with $B_0 = 0.1$ T/nm. The energy levels of the two qubit DCQ system are shown in Fig. 4. Dipole transition moments are tabulated in Table V; the Rabi oscillation periods are also tabulated for the electric field of $\mathcal{E}_0 = 10^5$ V/m. The transition dipole moments are large except for the transition between $|DU\rangle$ and $|UD\rangle$.

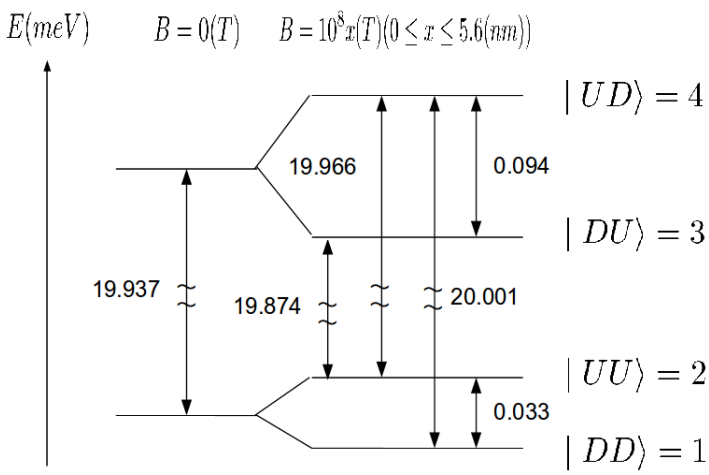

FIG. 4: Energy level of the two-qubit DCQ system.

TABLE II: Transition dipole moments and periods of Rabi oscillations for the two-qubit parallel DCQ system.

k	l	${\mu^y}_{kl}$ (10^{-30} Cm)	Rabi period (ns)
$\mid DD\rangle$	$\mid UU\rangle$	2.993	2.213
$\mid DD\rangle$	$\mid DU\rangle$	10.477	0.632
$\mid DD\rangle$	$\mid UD\rangle$	10.475	0.633
$\mid UU\rangle$	$\mid DU\rangle$	10.475	0.633
$\mid UU\rangle$	$\mid UD\rangle$	10.477	0.632
$\mid DU\rangle$	$\mid UD\rangle$	0.009	776.068

TABLE III: Transition dipole moments and the period of Rabi oscillations for the two-qubit PLCQ system.

k	l	${\mu^y}_{kl}(10^{-30}\mathrm{C}\cdot\mathrm{m})$	Rabi period(ns)	${\mu^x}_{kl}(10^{-30}\mathrm{C}\cdot\mathrm{m})$	Rabi period (ns)
$\mid R_S L_S\rangle$	$\mid L_S R_S\rangle$	1.211	5.472	0	1.497×10^{10}
$\mid R_S L_S\rangle$	$\mid R_S R_S\rangle$	6.873	0.964	0.049	134.298
$\mid R_S L_S\rangle$	$\mid L_S L_S\rangle$	6.87	0.965	0.049	134.298
$\mid L_S R_S\rangle$	$\mid R_S R_S\rangle$	6.87	0.965	0.049	134.298
$\mid L_S R_S\rangle$	$\mid L_S L_S\rangle$	6.873	0.964	0.049	134.298
$\mid R_S R_S\rangle$	$\mid L_S L_S\rangle$	0.044	152.293	0	3.346×10^8

We consider another two qubit system that has relatively large transition moments between all qubit states (Fig. 6). In this system, the current patterns look like a swinging pendulum in the left side and right side positions, so we call them Pendulum-Like-Current-Qubit (PLCQ). The state with the current look like the pendulum in the left side and right side are denoted as L_S and R_S, respectively.

The two qubit system of PLCQs is shown in Fig. 6. Energy levels in the magnetic field are shown in Fig. 8. Now some dipole transition moments have both x and y components; they may allow more flexible control of transitions.

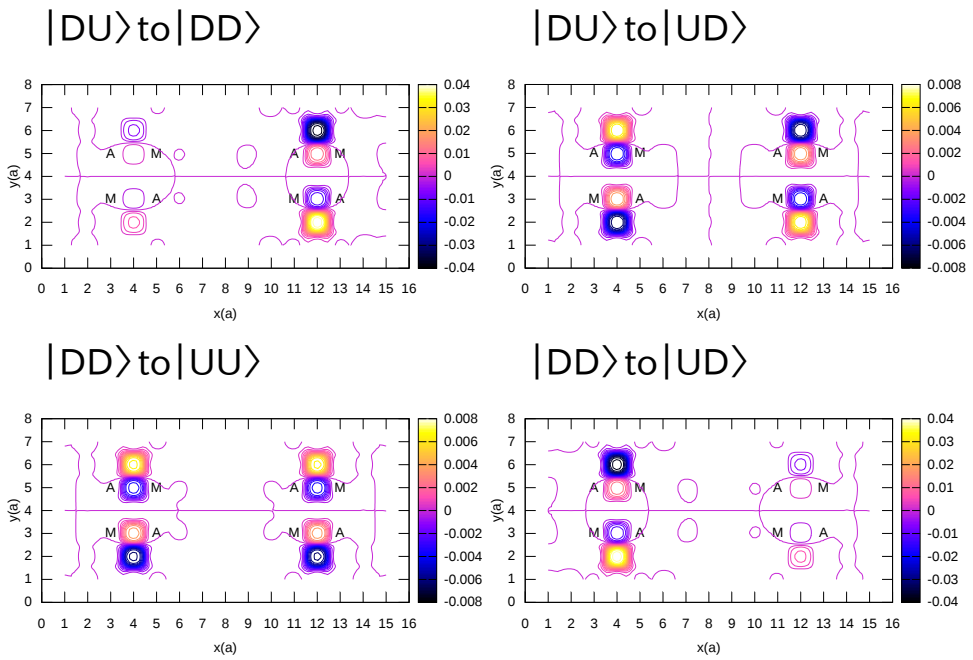

FIG. 5: Imaginary part of transition charge density divided by e for the two-qubit DCQ system. Real part is calculated to be zero.

VI. CONTROLLING SVILC QUBITS BY ELECTRIC DIPOLE TRANSITIONS

In this section, we discuss a method to control SVILC qubits using the electric dipole transition. As for the qubit system, we use the PLCQ system.

The time-dependent Schrödinger equation is expressed as

$$i\hbar\frac{\partial}{\partial t}|\Psi(t)\rangle = H(t)|\Psi(t)\rangle \tag{27}$$

where the Hamiltonian H is given by

$$H = H_0 + H_D. \tag{28}$$

For the zeroth order Hamiltonian, we use the following approximate one;

$$H_0 = H_{EHFS}^{HF} + H_B \approx \sum_j E_j|\Phi_j\rangle\langle\Phi_j| \tag{29}$$

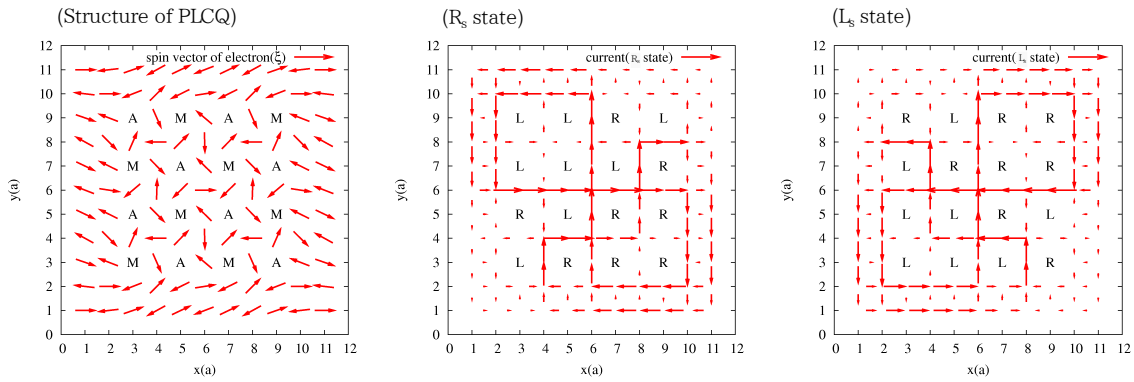

FIG. 6: The spin structure and current pattern of the PLCQ system. Left: the spin structure. Arrows indicate spin directions. 'M' and 'A' denote spin-vortices with $w_l[\xi] = 1$ and $w_l[\xi] = -1$, respectively. Middle: the current pattern for $|\ R_s\rangle$ state. Right: the current pattern for $|\ L_s\rangle$ state.

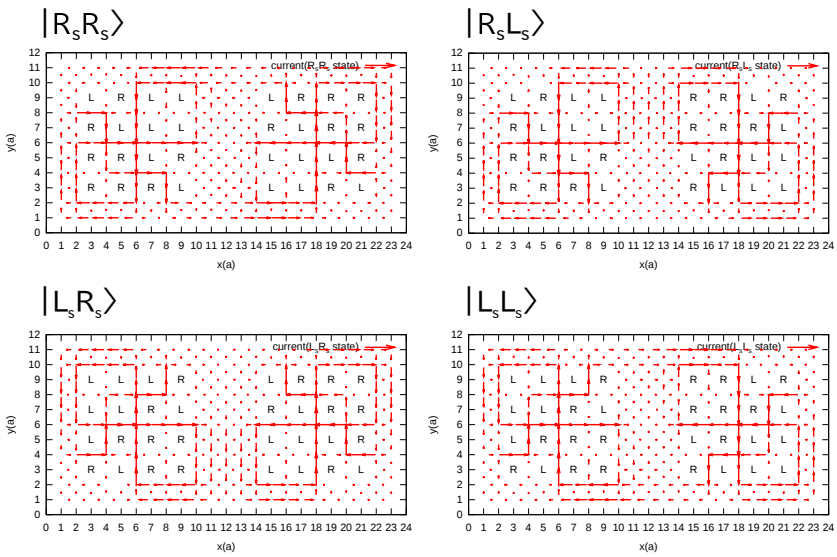

FIG. 7: Four current patterns for the two-qubit PLCQ system.

where E_j is the expectation value of energy for $|\Phi_j\rangle$ given by

$$E_j = \langle \Phi_j | H_0 | \Phi_j \rangle. \tag{30}$$

We expand the time-dependent state $|\Psi(t)\rangle$ as

$$|\Psi(t)\rangle = \sum_j b_j(t) |\Phi_j\rangle e^{-i\frac{E_j}{\hbar}}, \tag{31}$$

and solve the time-dependent equation for $b_j(t)$.

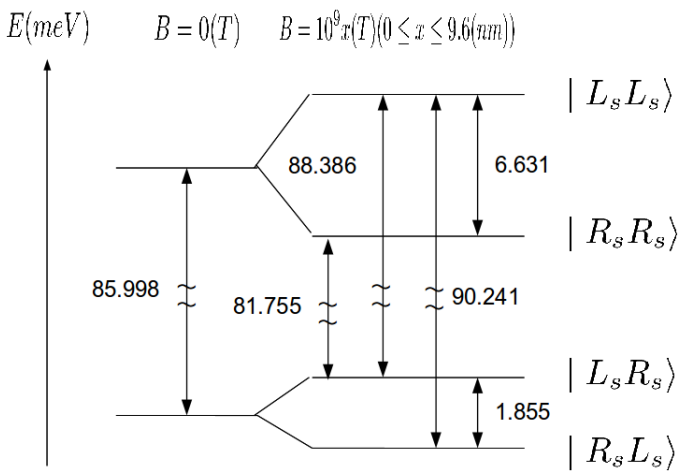

FIG. 8: Energy level of the two-qubit PLCQ system.

From Eq. (27), it is given by

$$i\hbar\dot{b}_k(t) = \sum_j M_{kj}(t)b_j(t) \tag{32}$$

where $M_{kj}(t)$ is defined as

$$M_{kj}(t) = \mathcal{E}_0\mu^y_{kj}\cos(\omega t + \phi)\exp(i\omega_{jk}t), \quad \omega_{jk} = \frac{E_j - E_k;}{\hbar} \tag{33}$$

here, we used the linearly polarized light in the y direction to realize Rabi oscillations. The equation (32) is solved by using the Chebychev series expansion method [24].

In order to describe quantum gates, we introduce the matrix expression for the time-evolution of the vector $\mathbf{b}^T(t) = (b_1(t), b_2(t), \cdots)$ ($\mathbf{b}^T$ is the transpose of $\mathbf{b}$) from $t = 0$ to $t = t_1$ as

$$\mathbf{b}(t_1) = P\mathbf{b}(0), \tag{34}$$

where the time-evolution matrix P is given by

$$P = \exp\left[-\frac{i}{\hbar}\int_0^{t_1} M(t')dt'\right]. \tag{35}$$

$M(t)$ is the matrix with elements $M_{kj}(t)$.

By irradiating the electromagnetic field with frequency $\omega = \omega_{\ell k} > 0$, the Rabi oscillation between $|\Phi_\ell\rangle$ and $|\Phi_k\rangle$ occurs. The time-evolution in this case is given by

$$P^{k\ell}(\theta,\phi) = \begin{pmatrix} \cos\frac{\theta}{2} & -i\frac{\mu_{k\ell}}{|\mu_{k\ell}|}e^{i\phi}\sin\frac{\theta}{2} \\ -i\frac{\mu^*_{k\ell}}{|\mu_{k\ell}|}e^{-i\phi}\sin\frac{\theta}{2} & \cos\frac{\theta}{2} \end{pmatrix} \tag{36}$$

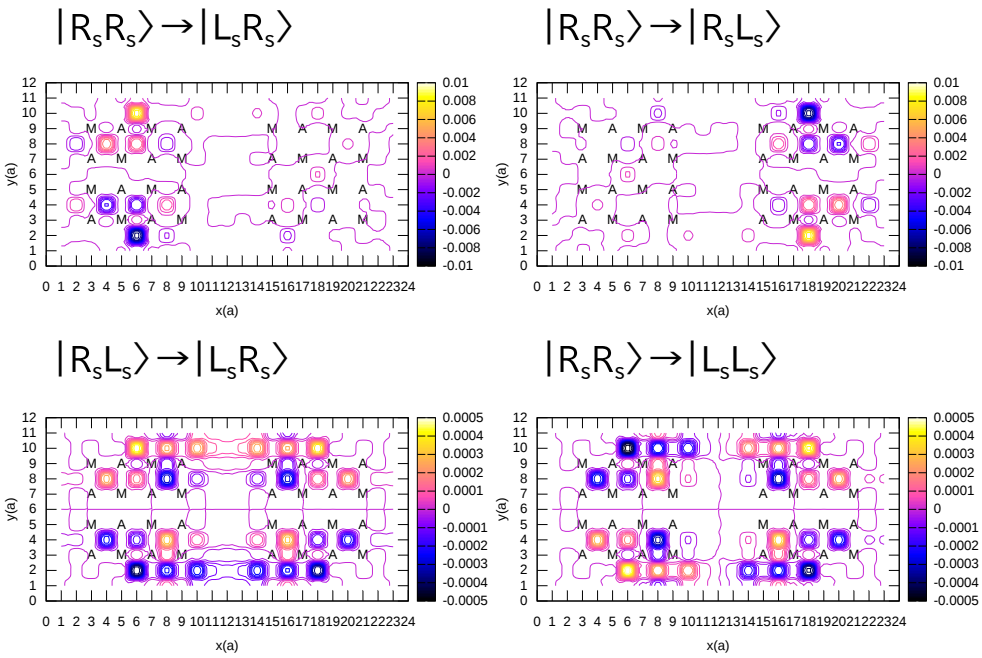

FIG. 9: Imaginary part of transition charge density divided by e for the two-qubit PLCQ system. Real part is zero.

where

$$\theta = \frac{2\pi}{T_{k\ell}} t_1 \tag{37}$$

with $T_{k\ell}$ being the period of Rabi oscillation given by

$$T_{k\ell} = \frac{h}{|\mu^y_{k\ell}| \mathcal{E}_0}. \tag{38}$$

In our calculation, we use the convention where transition moments are pure imaginary (i.e., $\mathrm{Re}\{\mu^y_{k\ell}\} = 0$).

For the basis for the two-qubit system we consider here, components b_0, b_1, b_2, and b_3 correspond to the coefficient of the basis $|R_S R_S\rangle \equiv |00\rangle$, $|R_S L_S\rangle \equiv |01\rangle$, $|L_S R_S\rangle \equiv |10\rangle$, and $|L_S L_S\rangle \equiv |11\rangle$, respectively.

The rotation operator $R_1(\theta,\phi)$ for the first qubit is given by

$$R(\theta,\phi)_1 = \begin{pmatrix} P^{13}(\theta,\epsilon^{13}\phi)_{11} & 0 & P^{13}(\theta,\epsilon^{13}\phi)_{12} & 0 \\ 0 & P^{24}(\theta,\epsilon^{24}\phi)_{11} & 0 & P^{24}(\theta,\epsilon^{24}\phi)_{12} \\ P^{13}(\theta,\epsilon_{13}\phi)_{21} & 0 & P^{13}(\theta,\epsilon^{13}\phi)_{22} & 0 \\ 0 & P^{24}(\theta,\epsilon^{24}\phi)_{21} & 0 & P^{24}(\theta,\epsilon^{24}\phi)_{22} \end{pmatrix}, \tag{39}$$

and that for the second qubit is given by

$$R(\theta,\phi)_2 = \begin{pmatrix} P^{12}(\theta,\epsilon^{12}\phi)_{11} & P^{12}(\theta,\epsilon^{12}\phi)_{12} & 0 & 0 \\ P^{12}(\theta,\epsilon^{12}\phi)_{21} & P^{12}(\theta,\epsilon^{22}\phi)_{12} & 0 & 0 \\ 0 & 0 & P^{34}(\theta,\epsilon^{34}\phi)_{11} & P^{34}(\theta,\epsilon^{34}\phi)_{12} \\ 0 & 0 & P^{34}(\theta,\epsilon^{34}\phi)_{21} & P^{34}(\theta,\epsilon^{34}\phi)_{22} \end{pmatrix}, \tag{40}$$

where ϵ^{jk} is defined as

$$\epsilon^{jk} = \begin{cases} +1 \ \text{ for } \mathrm{Im}(\mu_{jk}) > 0 \\ -1 \ \text{ for } \mathrm{Im}(\mu_{jk}) < 0 \end{cases} \tag{41}$$

The rotation around the x-axis by θ for the jth qubit is given by

$$R_{jx}(\theta) = -iR(\theta,\frac{\pi}{2})_j \tag{42}$$

and that around the z-axis is given by

$$R_{jz}(\theta) = H_j R_{jx}(\theta) H_j, \tag{43}$$

where H_j is the Hadamard gate for the jth qubit; the Pauli X, Y, Z gates, and the Hadamard gate Z for the jth qubit are given by

$$X_j = -iR\left(\pi,\frac{\pi}{2}\right)_j, \quad Y_j = -iR\left(\pi,-\pi\right)_j, \quad Z_j = H_j^{-1}X_jH_j, \quad H_j = -R\left(\frac{3\pi}{2},0\right)_j \tag{44}$$

Two-qubit gates such as Controlled-NOT(CNOT or CX) are also given as 4×4 matrices. They are depicted in Fig. 10, where the first qubit is used as the control gate.

Other gate operations are realized by the combinations of $R(\theta,\phi)$'s. The current gate operation method is not practical due to the fact that it requires additional tuning of relative phases between qubits since the interactions always exist between all qubits. In order to overcome this difficulty, couplers that can turn on/off interactions between qubits must be introduced. Actually, such couplers can be made by using external feeding currents.

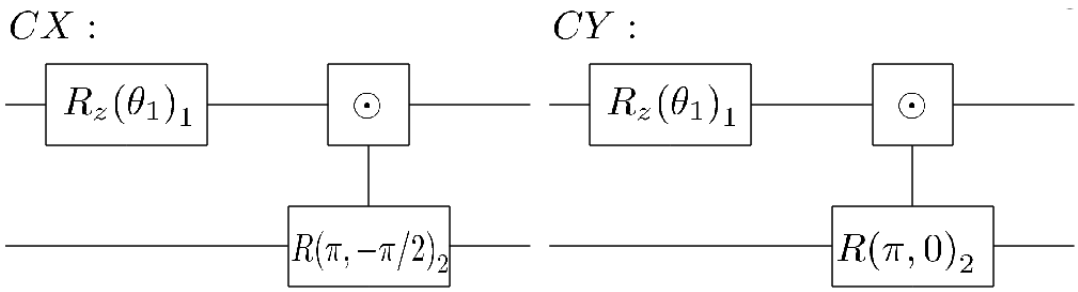

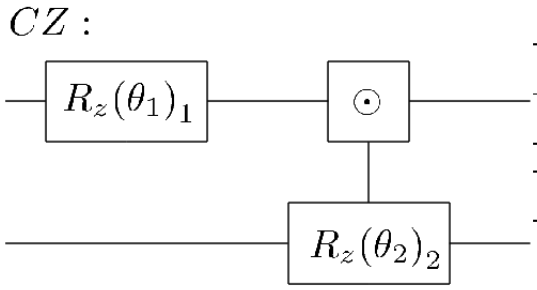

(a)	R_sR_s	R_sL_s	L_sR_s	L_sL_s
θ_1	$-\pi/2$	$\pi/2$	$-\pi/2$	$\pi/2$

(b)	R_sR_s	R_sL_s	L_sR_s	L_sL_s
$\odot$	$\circ$	$\cdot$	$\circ$	$\cdot$
θ_2	$-\pi$	$-\pi$	π	π

FIG. 10: Quantum circuit to demonstrate Controlled-NOT(CX), CY and CZ gate. Table (a) indicates the correspondence between rotation degree in left R_z gate and aimed state. Table (b) indicates the correspondence between the work of control qubit ('$\bullet$' indicates that the target operation is performed if the control qubit is 1, '$\circ$' does that if the control qubit is 0).

VII. SIMULATION OF GROVER'S SEARCH ALGORITHM

In this section, we demonstrate Grover's search algorithm using the two qubit system explained in the previous section. For that purpose we follow the work using the trapped atomic ion qubits [25]. Grover's search algorithm is a quantum search algorithm that speeds up a search through an unstructured elements. Main routine of this algorithm is to repeat amplifying the population of the solution state and suppress others by the so-called *Grover's operation*. It uses a quantum register for the elements $|x\rangle$ (x runs from integers 0 to $N-1$, where N is the total number of elements) and a qubit called the *oracle qubit* $|q\rangle$ to mark the solution state [26].

The oracle operation is defined by

$$|x\rangle|q\rangle \rightarrow |x\rangle|q \oplus f(x)\rangle \tag{45}$$

where $f(x) = 1$ if x is the solution of the search, and $f(x) = 0$ if x is not.

The oracle qubit is initially in $\frac{1}{\sqrt{2}}(|0\rangle - |1\rangle)$, thus, the oracle operation in Eq. (45) is given by

$$|x\rangle \frac{1}{\sqrt{2}}(|0\rangle - |1\rangle) \rightarrow (-1)^{f(x)}|x\rangle \frac{1}{\sqrt{2}}(|0\rangle - |1\rangle). \tag{46}$$

If the solution state is denoted by $|z_0\rangle$, the oracle operation in Eq. (46) is described using the operation on the data register $|x\rangle$ as

$$U(z_0) \mid x\rangle = \begin{cases} - \mid x\rangle, & x = z_0 \\ \mid x\rangle, & x \neq z_0, \end{cases} \tag{47}$$

i.e., it changes the sign of the target state.

The above operation is represented as

$$U(z_0) = I - 2 \mid z_0\rangle\langle z_0 \mid, \tag{48}$$

where I is the unit matrix. This $U(z_0)$ is one of the two operators needed to construct the *Grover's operator*.

The other operator is $U(\psi)$ given by

$$U(\psi) = I - \mid \psi\rangle\langle\psi \mid . \tag{49}$$

where $|\psi\rangle$ is the state defined by

$$|\psi\rangle = H^{\otimes n}|0\rangle = \frac{1}{\sqrt{2^n}} \sum_{x=0}^{2^n-1} |x\rangle \tag{50}$$

with $N = 2^n$ being the number of elements of the data.

Using $U(z_0)$ and $U(\psi)$, the *Grover's operator* is given by

$$U(G) = U(\psi)U(z_0). \tag{51}$$

In the following, we perform the Grover's search algorithm for $N = 4$ using the method described in Ref. [25]. In this case, one time application of $U(G)$ is enough for the search. In Fig. 11, the logical quantum circuits are depicted. The oracle operation is achieved by a Z gate and a Controlled-Z gate (CZ gate).

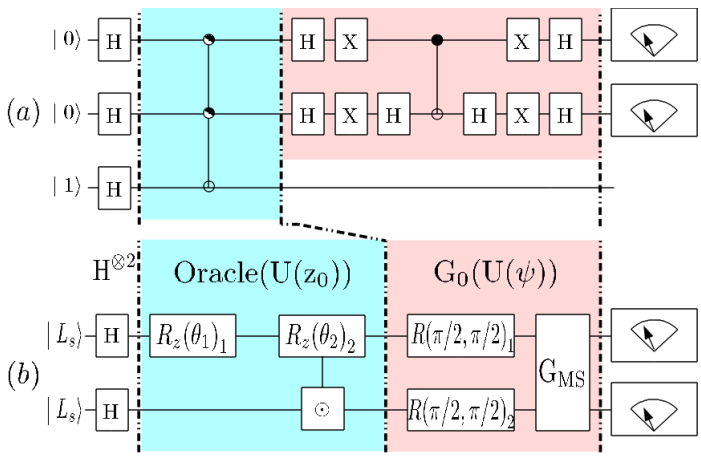

(c)	R_sR_s	R_sL_s	L_sR_s	L_sL_s
θ_1	$-\pi/2$	$\pi/2$	$-\pi/2$	$\pi/2$

(d)	R_sR_s	R_sL_s	L_sR_s	L_sL_s
$\odot$	$\circ$	$\cdot$	$\circ$	$\cdot$
θ_2	$-\pi$	$-\pi$	π	π

FIG. 11: Logical quantum circuits of Grover's algorithm for $N = 4$ elements (a) Logical quantum circuit using the oracle qubit: the first two qubits are the registry for elements. (b) Simulated logical quantum circuit without using the oracle qubit: $U(z_0)$ operation is done by a Z gate and a controlled Z gate (CZ gate). $U(\psi)$ operation is done by $R(\pi/2, \pi/2)$ on two qubits followed by Mølmer-Sørensen gate. R_s and L_s correspond to 0 and 1, respectively. Tables (c) and (d) denote operations to the oracle operations for various states.

$U(\psi)$ operation is done by $R(\pi/2, \pi/2)$ on each qubit followed by Mølmer-Sørensen gate defined as

$$G_{MS} = \frac{1}{\sqrt{2}} \begin{pmatrix} 1 & 0 & 0 & -\mathrm{i} \\ 0 & 1 & -\mathrm{i} & 0 \\ 0 & -\mathrm{i} & 1 & 0 \\ -\mathrm{i} & 0 & 0 & 1 \end{pmatrix} \tag{52}$$

In Fig. 12, the result of simulation is depicted. The search completes in a nanosecond scale using the electric field of the amplitude of $\mathcal{E}_0 = 10^5$ V/m.

VIII. CONCLUSION

In the present work, we have proposed new qubits, the *spin-vortex-induced loop current* (SVILC) qubits, that may satisfy all of the DiVincenzo's five criteria. Although the SVILC

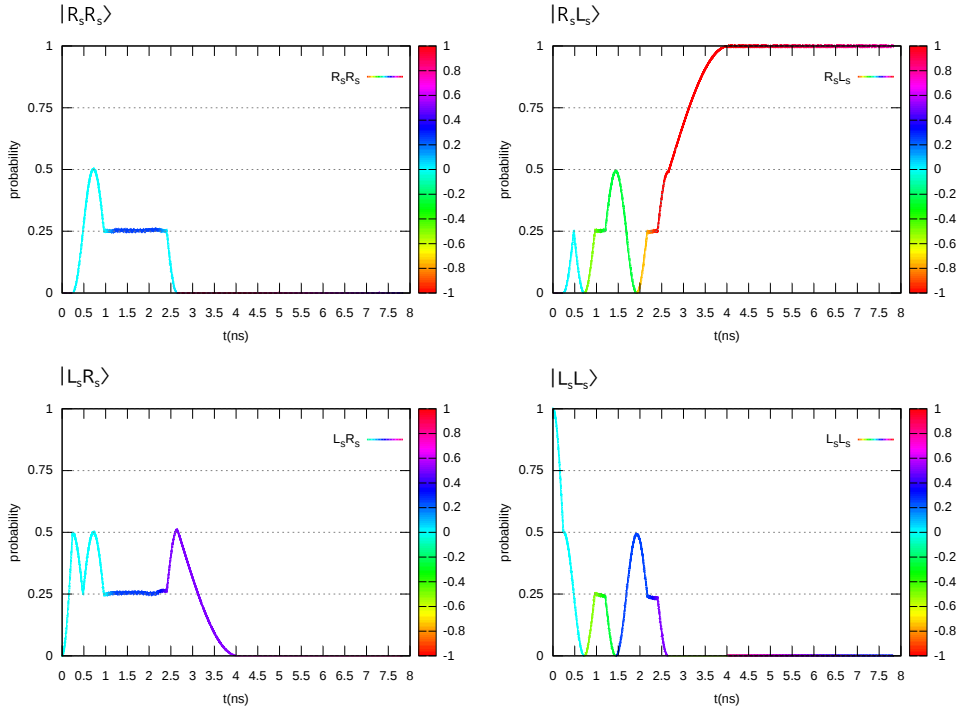

FIG. 12: The result of simulation that search $|R_sL_s\rangle$ state by Grover's search algorithm. Four plots represent population of each state with respect to elapsed time. The electric field amplitude $\mathcal{E}_0$ is 10^5 V/m for $t < 2.65$ ns, and 10^6 V/m for $t > 2.65$ ns (Since the dipole transition moments for the Mølmer-Sørensen gate operation are very small compared to those for other gate operations, we increase the amplitude of $\mathcal{E}_0$ by 10 for the Mølmer-Sørensen gate operation to speed up the simulation). The phase of each state is expressed as the color of line (1 and -1 mean π and $-\pi$, respectively). Application of Hadamard operations completes at 0.48 ns. Oracle operation completes at 2.17 ns. Mølmer-Sørensen gate starts at 2.65 ns.

is not detected experimentally so far, a number of experiments suggest its presence in the CuO_2 plane of the bulk of the cuprate. However, the experimental detection of the SVILC is desperately needed.

In the present theoretical investigation, we only extracted a single CuO_2 plane and used it. In reality, the effects of the other CuO_2 planes and intervening charge reservoir layers between them are not negligible. However, the present work has demonstrated the potentiality of the SVILC as qubit. Using parameters appropriate for the cuprate superconductor, the good quantum gate control capability of the SVILC qubits has been suggested; the calculated

transition dipole moments are large enough to perform the gate control in a nanosecond order by the irradiation of the electromagnetic field with the electric field amplitude of $\mathcal{E}_0 = 10^5$ V/m. Although, further researches are still needed, the SVILC qubit is a promising candidate for realizing practical quantum computers.

---

[1] M. Brune, F. Schmidt-Kaler, A. Maali, J. Dreyer, E. Hagley, J. M. Raimond, and S. Haroche, Phys. Rev. Lett. **76**, 1800 (1996).

[2] D. Leibfried, E. Knill, S. Seidelin, J. Britton, R. B. Blakestad, J. Chiaverini, D. B. Hume, W. M. Itano, J. D. Jost, C. Langer, et al., Nature **438**, 639 (2005).

[3] H. Häffner, W. Hänsel, C. F. Roos, J. Benhelm, D. Chek-al-kar, M. Chwalla, T. Körber, U. D. Rapol, M. Riebe, P. O. Schmidt, et al., Nature **438**, 643 (2005).

[4] J. Clarke and F. K. Wilhelm, Nature **453**, 1031 (2008).

[5] M. W. Johnson, M. H. S. Amin, S. Gildert, T. Lanting, F. Hamze, N. Dickson, R. Harris, A. J. Berkley, J. Johansson, P. Bunyk, et al., Nature **473**, 194 (2011).

[6] D. P. DiVincenzo, Fortschr. Phys. **48**, 771 (2000).

[7] R. Hidekata and H. Koizumi, J. Supercond. Nov. Magn. **24**, 2253 (2011).

[8] H. Koizumi, R. Hidekata, A. Okazaki, and M. Tachiki, J Supercond Nov Magn **27**, 121 (2014).

[9] H. Koizumi, A. Okazaki, M. Abou Ghantous, and M. Tachiki, J. Supercond. Nov. Magn. **27**, 2435 (2014).

[10] A. Okazaki, H. Wakaura, H. Koizumi, M. A. Ghantous, and M. Tachiki, J. Supercond. Nov. Magn. **28**, 3221 (2015).

[11] J. M. Tranquada, H. Woo, T. G. Perring, H. Goka, G. D. Gu, G. Xu, M. Fujita, and K. Yamada, Nature **429**, 534 (2004).

[12] S. A. Kivelson, I. P. Bindloss, E. Fradkin, V. Oganesyan, J. M. Tranquada, A. Kapitulnik, and C. Howald, Rev. Mod. Phys. **75**, 1201 (2003).

[13] J. Xia, E. Schemm, G. Deutscher, S. A. Kivelson, D. A. Bonn, W. H. Hardy, R. Liang, W. Siemons, G. Koster, M. M. Fejer, et al., Phys. Rev. Lett. **100**, 127002 (2008).

[14] Z. A. Xu, N. P. Ong, Y. Wang, T. Kakeshita, and S. Uchida, Nature **406**, 486 (2000).

[15] L. Mangin-Thro, Y. Sidis, A. Wildes, and P. Bourges, Nat. Commun. **6**, 7705 (2015).

[16] A. Bianconi, N. L. Saini, A. Lanzara, M. Missori, T. Rossetti, H. Oyanagi, H. Yamaguchi,

K. Oka, and T. Ito, Phys. Rev. Lett. **76**, 3412 (1996).

[17] S. Miyaki, K. Makoshi, and H. Koizumi, J. Phys. Soc. Jpn. **77**, 034702 (2008).

[18] Y. Kohsaka, T. Hanaguri, M. Azuma, M. Takano, J. C. Davis, and H. Takagi, Nature Phys. **8**, 534 (2012).

[19] V. J. Emery and S. A. Kivelson, Nature **374**, 434 (1995).

[20] H. Paik, D. I. Schuster, L. S. Bishop, G. Kirchmair, G. Catelani, A. P. Sears, B. R. Johnson, M. J. Reagor, L. Frunzio, L. I. Glazman, et al., Phys. Rev. Lett. **107**, 240501 (2011).

[21] P. W. Anderson, Phys. Rev **115**, 2 (1959).

[22] K. Yamaji, T. Yanagisawa, M. Miyazaki, and R. Kadono, J. Phys. Soc. Jpn. **80**, 083702 (2011).

[23] C. A. Mead and D. G. Truhlar, J. Chem. Phys. **70**, 2284 (1979).

[24] Tal - Ezer and R. Kosloff, J. Chem. Phys. **81**, 3967 (1984).

[25] K.-A. Brickman, P. C. Haljan, P. J. Lee, M. Acton, L. Deslauriers, and C. Monroe, Phys Rev. A **72**, 050306 (2005).

[26] L. K. Grover, Phys. Rev. Lett. **79**, 325 (1997).